Vibrational dynamics of the host framework in Sn clathrates

Bogdan M. Leu,[1,*] Mihai Sturza,[2] Michael Y. Hu,[1] David Gosztola,[3] Volodymyr Baran,[4] Thomas F. Fässler,[4] and E. Ercan Alp[1]

[1]*Advanced Photon Source, Argonne National Laboratory, Argonne, Illinois, USA*

[2]*Materials Science Division, Argonne National Laboratory, Argonne, Illinois, USA*

[3]*Center for Nanoscale Materials, Argonne National Laboratory, Argonne, Illinois, USA*

[4]*Department of Chemistry, Technische Universität München, Garching, Germany*

(Received 27 August 2014; revised manuscript received 3 September 2014; published 16 September 2014)

We use nuclear resonance inelastic x-ray scattering (NRIXS), a relatively new, synchrotron-based, isotope-specific technique in combination with a more traditional one, Raman spectroscopy, to probe the vibrational dynamics of the host frameworks in two Zintl clathrates: $K_8Zn_4Sn_{42}$ (KZS) and $Ba_8Ga_{16}Sn_{30}$ (BGS). From the *normalized* Sn vibrational density of states obtained from NRIXS, we calculate the stiffness, a mean force constant of the Sn environment, the resilience, a compact way of expressing the temperature dependence of the Sn mean square displacement, and several thermodynamic properties. The stiffness and the resilience are approximately 7% lower in KZS, reflecting its larger unit cell compared to BGS. We emphasize the complementariness between NRIXS and Raman spectroscopy and establish a series of benchmarks for a more quantitative evaluation of the Raman spectra for the numerous clathrates that are still not suitable for NRIXS studies.

DOI: 10.1103/PhysRevB.90.104304 PACS number(s): 63.20.Pw

I. INTRODUCTION

Clathrates are compounds with beautiful structures consisting of (guest) atoms trapped inside (host) polyhedral cages [1] known for their thermoelectric [2], mechanical [3], magnetic [4], superconducting [5], and photovoltaic [6] properties. The close relationship between structure and properties is of scientific and technological importance [7,8]. Among other applications, clathrates are promising candidates in the search for new materials fitting the "phonon glass, electron crystal" concept, in which the phonon free paths are as short as possible while electron mean free paths are as long as possible [9]. Early studies associated the low thermal conductivities in a number of materials with the presence of loose, "rattling" atoms [10,11], hence the initial interest in probing the dynamics of the guest atoms in clathrates with a variety of techniques such as diffraction [12], nuclear resonant inelastic x-ray scattering [13], and inelastic neutron scattering [14]. On the other hand, the role played by the host framework occupancy and dynamics on the behavior of the guest atoms and, ultimately, on the thermal conductivity has been demonstrated both theoretically [15,16] and experimentally [17,18].

Improvement of thermoelectric materials in general requires a detailed knowledge of all the factors influencing their properties [19]. Hence, for clathrates it is of interest to probe the atomic dynamics of the host framework separately from that of the guest atoms and to extract mechanical and thermodynamic properties associated with it. Phonons, which are also important in understanding the superconducting mechanism [8,20], are usually studied with Raman spectroscopy [8,21,22] and inelastic neutron scattering (INS) [17,18,23]. With these techniques, however, is sometimes difficult to separate the contributions from the guest and the host atoms to the measured signal. (This separation can be accomplished, for example, by using isotope labeling in Raman [8] or the complementary techniques INS and inelastic x-ray scattering [23].) Nuclear resonance inelastic x-ray scattering [24,25] (NRIXS; other names used for this technique include nuclear inelastic scattering [13], nuclear resonance vibrational spectroscopy [26], and others) circumvents this difficulty due to its ultimate site selectiveness: it is an isotope-specific technique, with only the targeted atom(s) contributing to the measured spectrum. While ^{57}Fe is by far the most studied isotope, due to the importance of iron in biology, geophysics, and condensed matter physics, several other isotopes are suitable for NRIXS, such as ^{119}Sn, ^{151}Eu, ^{81}Kr, ^{149}Sm, ^{161}Dy, and ^{121}Sb. NRIXS has been used previously in investigations on Zintl and hydrate clathrates, in which the guest atoms—Eu [13] and Kr [27,28], respectively—were targeted. On the other hand, NRIXS studies on filled skutterudites (a related class of thermoelectric materials) helped elucidate the contribution of the host framework, in addition to that of the filler, to the lattice thermal conductivity in a series of experiments probing different (Fe, Sb) sites [29,30]. To the best of our knowledge, so far NRIXS has not been applied to probe the dynamics of the host framework in clathrates.

Here, we use Sn-based NRIXS to investigate the host framework dynamics in two promising thermoelectric materials: $K_8Zn_4Sn_{42}$ (KZS) and $Ba_8Ga_{16}Sn_{30}$ (BGS). KZS [31] (Fig. 1) is a type-I clathrate [2,32] (i.e., it consists of pentagonal dodecahedra and tetrakaidecahedra alternating in a 1:3 ratio) while BGS [18,33] (Fig. 2) is of type VIII (i.e., it contains only pentagonal dodecahedra; however, BGS adopts the type-I clathrate structure in the high-temperature modification [35]). Both have cubic unit cells, with $a = 12.071$ Å and space group $Pm\text{-}3n$ for KZS [31], and $a = 11.572$ Å and space group $I\text{-}43m$ for BGS [33,34].

We carried out parallel Raman measurements that revealed a remarkable complementariness between the two techniques. Differently from Raman spectroscopy however, NRIXS is an outstandingly quantitative technique, allowing us to extract the overall stiffness of the host framework and other parameters, and to establish a series of benchmarks in a Raman spectrum that may be useful for those compounds that are not suitable for NRIXS measurements.

*leu@aps.anl.gov

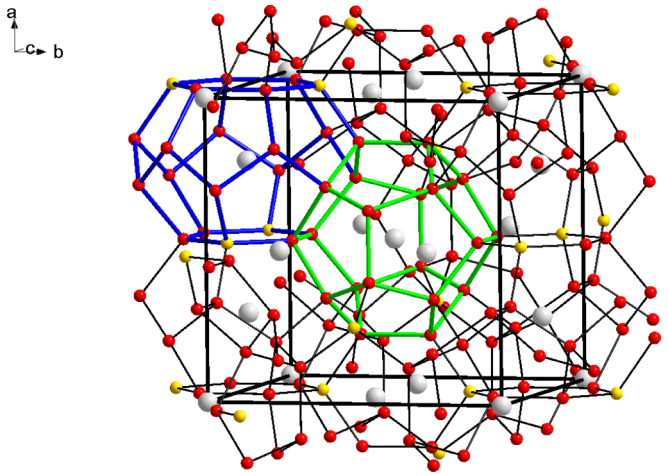

FIG. 1. (Color online) Structure of type-I clathrate $K_8Zn_4Sn_{42}$. Color scheme: gray = K, yellow = Zn/Sn, red = Sn. One small (pentagonal dodecahedron) and large (tetrakaidecahedron) host framework cage are highlighted in green and blue, respectively.

II. MATERIALS AND METHODS

A. Sample preparation

Single crystals of KZS and BGS were grown by a self-flux method using tin metal [33]. High-purity K, Zn powder, and Sn in the ratio of 4:2:63 were placed in a tantalum ampoule, which was sealed and heated with a rate of 1 K/min to 650 °C. The ampoule was held at this temperature for 1 h, followed by cooling to 200 °C with a rate of 0.1 K/min and to room temperature with a rate of 1 K/min. A carbon coated quartz tube containing high-purity Ba, Ga, and Sn mixed in an atomic ratio of 8:16:80 was evacuated and sealed under vacuum. The tube was placed in a computer-controlled furnace and was heated to 1100 °C over 12 h. The tube was kept at this temperature for 5 h and was subsequently cooled to room temperature in two steps: fast cooled to 500 °C and kept at this temperature for 18 h, then slowly cooled down to room temperature at a rate of 5 °C/h. Further details about sample preparation and characterization can be found in Refs. [31,34].

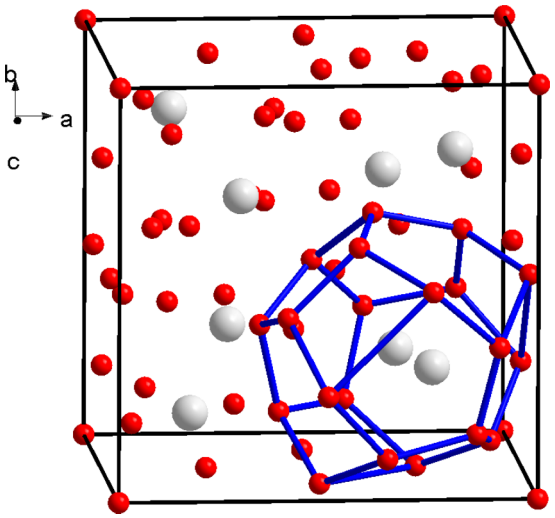

FIG. 2. (Color online) Structure of type-VIII clathrate $Ba_8Ga_{16}Sn_{30}$. Color scheme: gray = Ba, red = Sn/Ga. One host framework cage (pentagonal dodecahedron) is highlighted in blue.

B. Raman experiment

The measurements were performed at the Center for Nanoscale Materials, Argonne National Laboratory. Spectra were recorded at room temperature using 633-nm excitation from a helium-neon laser with 0.5-mW incident power and a Raman microscope (inVia Reflex, Renishaw, Inc.). Scattered light was collected through a 50X objective (Leica, NA = 0.75). The spectra are the result of averaging thirty 15-second integrations for KZS and ten 30-second integrations for BGS.

C. NRIXS experiment

NRIXS measurements were carried out at beamline 30-ID of the Advanced Photon Source (APS), Argonne National Laboratory. The incident monochromatic 23.88-keV x rays impinging on the sample had a flux of $\sim 1.7 \times 10^9$ Hz. The experimental resolution, obtained from a cryogenically-cooled, six-bounce high-resolution monochromator [36] was 1.3 meV (10.4 cm^{-1}). Energy scans, done at room temperature, covered the range from −40 to 70 meV with a 0.25 meV step. Multiple scans were added to obtain the data shown in Figs. S2 and S3 (panel A), Ref. [34], for a total collection time of ∼1.5 h for KZS and ∼4.5 h for BGS. Both samples contained naturally abundant Sn.

This work represents the first NRIXS project conducted at the 30-ID beamline, otherwise hosting the HERIX instrument, dedicated to the high-energy resolution inelastic x-ray scattering technique. The closeness between the operating energy for HERIX (23.724 keV) and for Sn-based NRIXS (23.88 keV) allows for the use of the same high-resolution monochromator for the two techniques. At the APS, ^{119}Sn NRIXS can be performed at beamline 3-ID as well [37,38] using a four-bounce, "nested" high-resolution monochromator [39].

The measured NRIXS signal (Figs. S2 and S3, panel A, Ref. [34]) consists of a central peak due to the recoilless excitation of the ^{119}Sn nucleus at $E_0 = 23.88$ keV and a series of sidebands of frequency $\bar{\nu}$ shifted with respect to E_0 by $hc\bar{\nu}$. The raw data was processed using Lipkin's first momentum sum rule [40] to produce a normalized excitation probability (Figs. S2 and S3, panel B, Ref. [34]). Program PHOENIX [41] was used to find the partial density of states $D(E)$ (Figs. S2 and S3, panel C, Ref. [34]) from the one-phonon contribution to the excitation probability (Figs. S2 and S3, panel B, Ref. [34]). Further details about NRIXS experiments in general and data analysis can be found elsewhere [24–26].

III. RESULTS AND DISCUSSION

The Raman spectra of KZS and BGS are shown in Fig. 3. The main bands are listed in Table I. Similar to previous experimental [16,21,22,42–44] and theoretical [16] Raman studies on Sn-containing clathrates, two main regions can be distinguished in the KZS and BGS spectra: around 60–80 cm^{-1} and above 150 cm^{-1}. Traditionally, the modes below 40 cm^{-1}

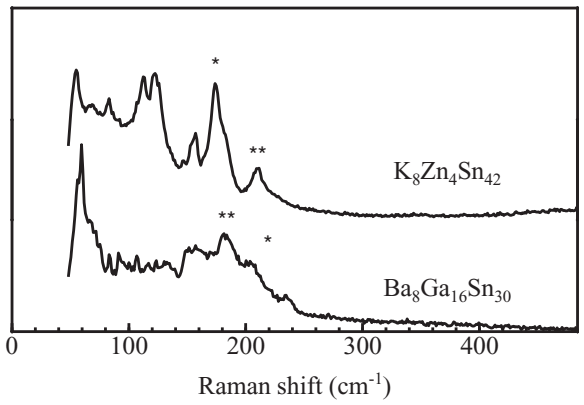

FIG. 3. Raman spectra for KZS and BGS. The frequencies of the peaks marked with * and ** are plotted in Fig. 4.

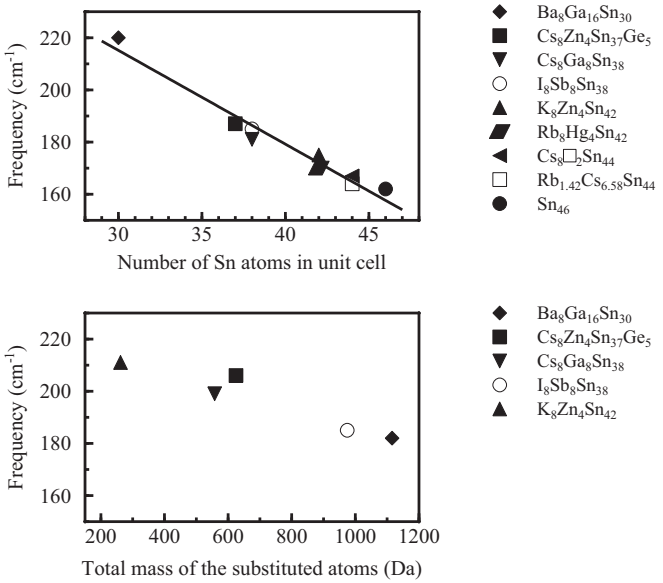

FIG. 4. (Top) Dependence of the frequency of the peaks marked with an asterisk in Fig. 3 on the number of the Sn atoms in the unit cell. (Bottom) Dependence of the frequency of the peaks marked with a double asterisk in Fig. 3 on the total mass of the substituted elements in the framework. Data for KZS (up triangle) and BGS (diamond) are from this work. The references for the other compounds are given in the text.

have been assigned as guest modes and those starting at slightly higher frequencies as framework modes, mostly due to the Sn atoms [16]. While the KZS and BGS Raman spectra are somewhat similar qualitatively, two particular differences are readily noticeable: first, the 80–150 cm^{-1} region in KZS is significantly richer than in BGS; second, the bands in the 180–230 cm^{-1} region in BGS are broader than in KZS, reminiscent of the broadening due to the presence of vacancies in related compounds [21]. Interestingly, minute vacancies in BGS have been recently reported from a combination of x-ray and neutron diffraction measurements [18]. Differences might also occur due to the different symmetries of the two compounds (different space groups). A recent theoretical study on BGS [45] agrees well with the experiment by predicting Raman active modes around 60 cm^{-1} and in the 100–165 cm^{-1} region. The high-frequency modes are shifting to lower frequencies in the calculation, likely a reflection of the larger predicted lattice constant with respect to the experimental value.

It is tempting to assign a one-to-one correspondence between the bands in the high-frequency regions of the two spectra (e.g., 183 cm^{-1} in KZS to 182 cm^{-1} in BGS; 211 cm^{-1} in KZS to 204 cm^{-1} in BGS, etc.). However, a look at the spectra of related compounds available in the literature (to the best of our knowledge, Raman measurements on KZS and BGS have not been reported), such as $Cs_8Zn_4Sn_{37}Ge_5$, $Cs_8Ga_8Sn_{38}$ [42], $I_8Sb_8Sn_{38}$, $Rb_8Hg_4Sn_{42}$, $Cs_8\square_2Sn_{44}$ [44]

TABLE I. Raman and NRIXS bands for KZS and BGS (in cm^{-1}).

Raman KZS	Raman BGS	NRIXS KZS	NRIXS BGS
		30	33
		43	45
55	59	56	64
68	67		
83		86	
111		111	109
122		134	131
157	148/157	160	158
175/183	182	181	173
211	204	214	193
	235		220

($\square$ = vacancy), $Rb_{1.42}Cs_{6.58}Sn_{44}$ [22], and Sn_{46} [16] (a theoretical study), presents a different picture. Specifically, it appears that the 180–230 cm^{-1} region is strongly influenced by the number of the Sn atoms in the unit cell (Fig. 4, top panel; for BGS, due to the rather broad Raman spectrum in this region, we included the value from NRIXS, 220 cm^{-1}) and by the total mass of the substituted elements present in the framework (Fig. 4, bottom panel). The former dependence is almost linear for the range considered:

$$\bar{\nu}(cm^{-1}) = -3.6 \times N + 323, \quad (1)$$

where $\bar{\nu}$ are the frequencies of the bands marked with an asterisk in Fig. 3 and N is the number of the Sn atoms in the unit cell. The latter tendency is also evident and well-documented. Bands around 200 cm^{-1}, which are absent in the Sn_{46} theoretical calculation, have been assigned to vibrations of the Ga atoms present in the framework of $Cs_8Ga_8Sn_{38}$ [16]. It should be noted that the corresponding bands in Ge-containing clathrates have higher frequencies [42], consistent with the higher mass of the Sn atoms compared to the Ge ones. Based on these results, we assign the bands marked with a double asterisk in Fig. 3 to vibrations due mainly to the Zn and Ga atoms in KZS and BGS, respectively.

Guest modes have very low frequencies [16,21,42,43], a region which we did not access in this study. (We note, however, that a peak with a frequency as high as 252 cm^{-1} was assigned as a Ba mode in Ba_8Si_{46} [8].) Framework vibrations appear at slightly higher frequencies ~50 cm^{-1}, with possible mixtures between guest atoms and framework vibrations having been reported [16]. Despite being very close to the cutoff in our experiment, it is evident that the strong 55-cm^{-1}

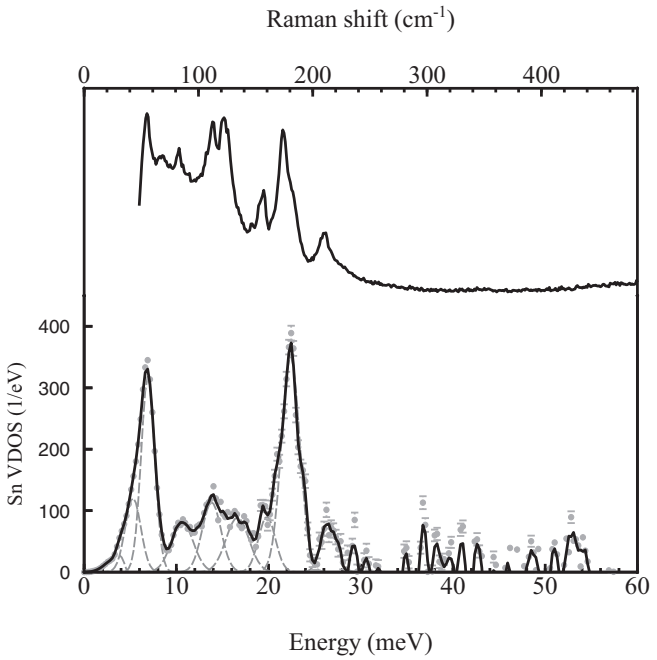

FIG. 5. Raman (top) and NRIXS (Sn VDOS, bottom) spectra for KZS. NRIXS data points are shown as markers with error bars, while the solid curve represents three-point running average. The individual peaks are shown as gray dashed lines. Their frequencies are listed in Table I.

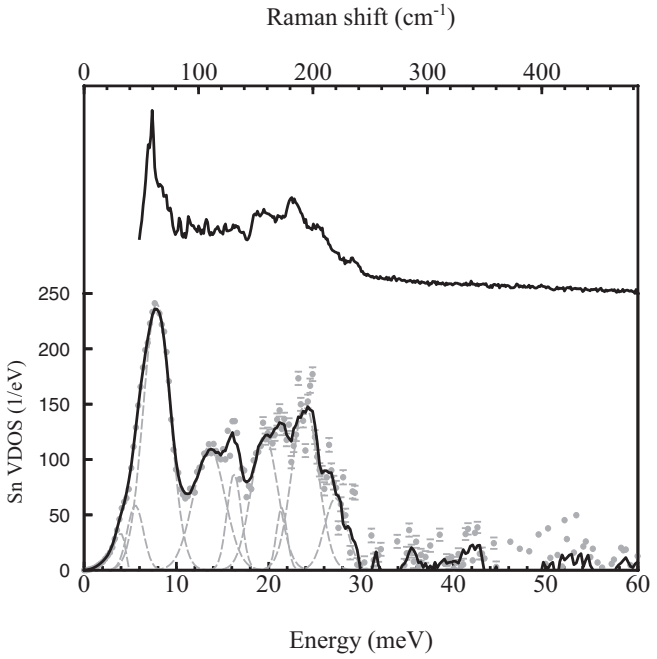

FIG. 6. Raman (top) and NRIXS (Sn VDOS, bottom) spectra for BGS. NRIXS data points are shown as markers with error bars, while the solid curve represents five-point running average. The individual peaks are shown as gray dashed lines. Their frequencies are listed in Table I.

band in KZS is shifting to higher frequencies in BGS (Fig. 3), consistent with the lighter $Ga_{16}Sn_{30}$ framework compared to the Zn_4Sn_{42} one. Such a dependence on the framework mass can be noticed in previous studies as well (e.g., $Ga_{16}Ge_{30}$ versus Ga_8Sn_{38}) [42]. To summarize the Raman discussion, the two regions with prominent features are sensitive to the number of Sn atoms in the unit cell and to the nature of the substituted atoms in the framework (high-frequency region, 180–230 cm^{-1}), and to the overall mass of the framework (low-frequency region, around 60 cm^{-1}).

Among the clathrate forming elements in the periodic table [1], three isotopes are suitable for routine NRIXS measurements: ^{151}Eu [29], ^{119}Sn [38], and ^{121}Sb [46]. Due to its isotope-selectiveness, NRIXS is an ideal tool for separating the guest and host framework contributions to the density of states that can be obtained from inelastic neutron scattering measurements [18]. Indeed, NRIXS has been used previously to probe the vibrational dynamics of the "rattling" Eu *guest* atoms in $Eu_8Ga_{16}Ge_{30}$ [13], but, to the best of our knowledge, has never been applied to target the *host* framework in clathrates.

To facilitate the following discussion, we plot together the Raman and NRIXS (Sn VDOS) spectra for KZS and BGS in Figs. 5 and 6, respectively. The lower panels also include the individual peaks (Gaussians, with the exception of the lowest-frequency one, which is log-normal; their frequencies are listed in Table I). For the sake of clarity, the fitting results, which match almost perfectly the averaged curves in Figs. 5 and 6, are not shown. The raw NRIXS spectra, the resolution function, the normalized spectra, and the one- and multi-phonon contributions are shown in Figs. S2 and S3 of Ref. [34].

Common Raman and NRIXS bands have been observed before [47–49]. In the present study however, the predominance of Sn atoms in the compounds investigated leads to remarkable, uncommon similarities between the Raman and NRIXS spectra, both for KZS and BGS. Like in the theoretical results for guest-free Sn_{46} [16], two regions with a higher concentration of density of states are noticeable: between 30 and 80 cm^{-1} (≈3.7–10 meV) and between 160 and 200 cm^{-1} (≈20–25 meV). No signal, other than due to statistical fluctuations, is present above 240 cm^{-1}, consistent with the Raman spectra and with previous Raman studies on Sn-containing clathrates. For KZS, an almost perfect one-to-one correspondence can be achieved between the Raman and NRIXS bands (Fig. 5, Table I). Two possible exceptions are the weak 68 cm^{-1} Raman band, which may be hidden by the neighboring strong 55-cm^{-1} NRIXS peak and the 134-cm^{-1} NRIXS band, which may be Raman inactive.

Good agreement between the results produced by the two experiments exists for BGS as well (Fig. 6), although the weak, featureless 80–140 cm^{-1} region and the broader bands above 140 cm^{-1} make a one-to-one connection between the two spectra somewhat harder to obtain, compared to KZS. Nevertheless, both the dominant 60–80 cm^{-1} peaks and the 140–230 cm^{-1} feature in the Raman spectrum are clearly reproduced in the Sn VDOS obtained from NRIXS. The slight shift of the strong 55-cm^{-1} Raman band in KZS to 59 cm^{-1} in BGS is also reproduced by NRIXS (Figs. 5 and 6). Evidently, NRIXS does not directly probe the dynamics of the

substituted atoms in the two compounds. However, vibrations of the neighboring Sn atoms accompany those of the Zn and Ga atoms, thus leaving a footprint in the Sn VDOS (∼211 cm^{-1} in KZS, ∼182 cm^{-1} in BGS).

Since NRIXS targets only the Sn atoms, the almost identical spectra obtained from the two experiments for both compounds suggest that the frameworks (Sn atoms in particular) dominate the Raman spectra in the region investigated. Contributions from the K and Ba atoms are nevertheless expected, similar to the mixture between guest atom and framework vibrations previously reported for a related compound [16]. This expectation is confirmed by the Eu-based NRIXS study on $Eu_8Ga_{16}Ge_{30}$ by Hermann and coworkers, in which the partial VDOS of the guest atoms extends up to approximately 70 cm^{-1}. The significant overlap between the Eu VDOS [13] and Sn VDOS (this work) in the 40–70 cm^{-1} region unambiguously demonstrates that the low-frequency vibrations cannot be rigidly assigned to either guest or host vibrations, but rather to a combination of the two. This comparison underscores the complementariness between the two NRIXS studies on Zintl clathrates to date, in spite of the differences between the structures of the three materials: (Ga,Ge) versus (Zn/Ga, Sn) frameworks; Eu versus K/Ba guest atoms.

Compared to Raman spectroscopy, NRIXS is a highly quantitative technique. From the partial (Sn in this study) VDOS numerous thermodynamic and elastic parameters can be calculated [24,25,50,51]. We begin by considering the vibrational component of the mean square displacement (msd) along the incident photon direction $\langle z^2\rangle_v$, given by

$$\langle z^2\rangle_v = \frac{1}{3k^2}\int [2\bar{n}(\bar{\nu})+1]\,\frac{\bar{\nu}_R}{\bar{\nu}}D(\bar{\nu})d\bar{\nu}, \qquad (2)$$

in which $D(\bar{\nu})$ is the Sn VDOS, $hc\bar{\nu}_R = \hbar^2k^2/2m_j$ is the recoil energy of a free nucleus of mass m_j absorbing a photon of energy $E = \hbar ck$, and $\bar{n} = [\exp(hc\bar{\nu}/k_BT)-1]^{-1}$ represents the mean occupation number of mode $\bar{\nu}$ at temperature T (k_B is the Boltzmann constant). In this study, $\bar{\nu}_R = 20.76\ cm^{-1}$ (the photon energy changes only ±70 meV with respect to the nuclear excitation energy $E_0 = 23.88$ keV), $k = 12.1\ Å^{-1}$ is the magnitude of the wave vector of the absorbed photon, and $\int D(\bar{\nu})d\bar{\nu} = 3$. The $\langle z^2\rangle_v$ values at 298 K for KZS and BGS (0.0115 and 0.0106 $Å^2$, respectively) are much smaller than those obtained from diffraction [31,33], as previously reported for skutterudites as well [30].

It should be noted here that, like in other Sn-based NRIXS measurements at room temperature [37,38], multiphonon contributions are quite significant in both KZS and BGS (Fig. S2 and S3, panel B, Ref. [34]), leading to somewhat low values (0.19 for KZS, 0.21 for BGS) for the Lamb-Mössbauer factor (or recoilless fraction) $f_{LM} = \exp(-k^2 < z^2 >_v)$. If f_{LM} becomes too low, the VDOS cannot be extracted [52].

At sufficiently high temperatures, $k_BT \gg hc\bar{\nu}$, the msd depend linearly on temperature [53]:

$$\langle z^2\rangle_{HT} = T\frac{2\bar{\nu}_Rk_B}{3hck^2}\int \frac{D(\bar{\nu})}{\bar{\nu}^2}d\bar{\nu}. \qquad (3)$$

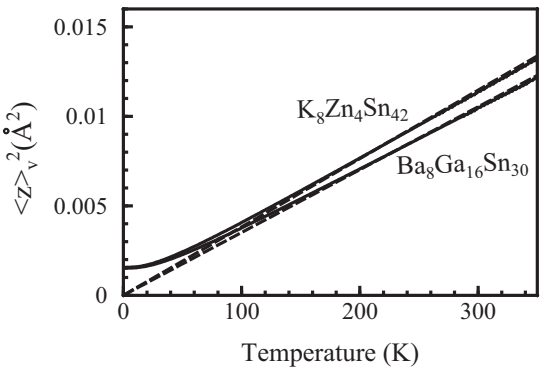

FIG. 7. Temperature dependence of the vibrational contribution to the Sn msd extrapolated from the Sn VDOS measured at a single temperature from Eq. (2). Dashed lines represent the high-temperature slopes determined from Eq. (3).

On the other hand, $\langle z^2\rangle_v$ does not vanish as $T \to 0$, but approaches a finite value given by [53]

$$\langle z^2\rangle_0 = \frac{\bar{\nu}_R}{3k^2}\int \frac{D(\bar{\nu})}{\bar{\nu}}d\bar{\nu}. \qquad (4)$$

A comparison between these extreme cases yields a temperature T^* at which the high-temperature msd [Eq. (3)] first exceeds the zero-point motion [Eq. (4)]. The T^* values for the two compounds are 42 K for KZS and 44 K for BGS.

Using Eq. (2), we extrapolated the temperature dependence of the vibrational contribution to the msd for KZS and BGS from the Sn VDOS measured at a single temperature (continuous lines in Fig. 7). The limiting high-temperature slopes Eq. (3) are indicated as dashed lines. Their values are 3.8×10^{-5} $Å^2/K$ for KZS and 3.5×10^{-5} $Å^2/K$ for BGS.

As seen above, the msd depend strongly on temperature. The concept of resilience [54],

$$k_r = \frac{k_B}{d < z^2 > /dT}, \qquad (5)$$

was introduced to describe in a compact way the temperature dependence of the atomic fluctuations in proteins when this dependence is approximately linear. Therefore the VDOS obtained from NRIXS measurements at a single temperature yields the resilience of the Sn framework [Eqs. (3) and (5)]. The k_r values for KZS and BGS are 36.4 and 39.5 N/m, respectively. The slightly stronger temperature dependence for KZS with respect to BGS (Fig. 7) can be explained by an increased Sn VDOS integrated area for the former below approximately 65 cm^{-1} [Fig. 8(a)].

In Fig. 8, we plot the quantities $D(\bar{\nu})/\bar{\nu}$ [panel (b)] and $D(\bar{\nu})/\bar{\nu}^2$ [panel (c)] as a function of frequency. The modes below 90 cm^{-1} represent 85% of the integrated area of $D(\bar{\nu})/\bar{\nu}^2$ for KZS and 84% for BGS, while they contribute only 63% and 62%, respectively, to the integrated area of $D(\bar{\nu})/\bar{\nu}$ in the same range. These results indicate that low-frequency vibrations dominate the high-temperature behavior of the Sn msd [Eq. (3)], while the full spectrum contributes to the zero-point motion [Eq. (4)]. Not surprisingly, the shift of the 55 cm^{-1} Raman band in KZS (Fig. 3, Table I) by ∼4 cm^{-1} in BGS not only that is reflected in the Sn VDOS of the respective compounds [Fig. 8(a)], but it leads to a noticeable difference

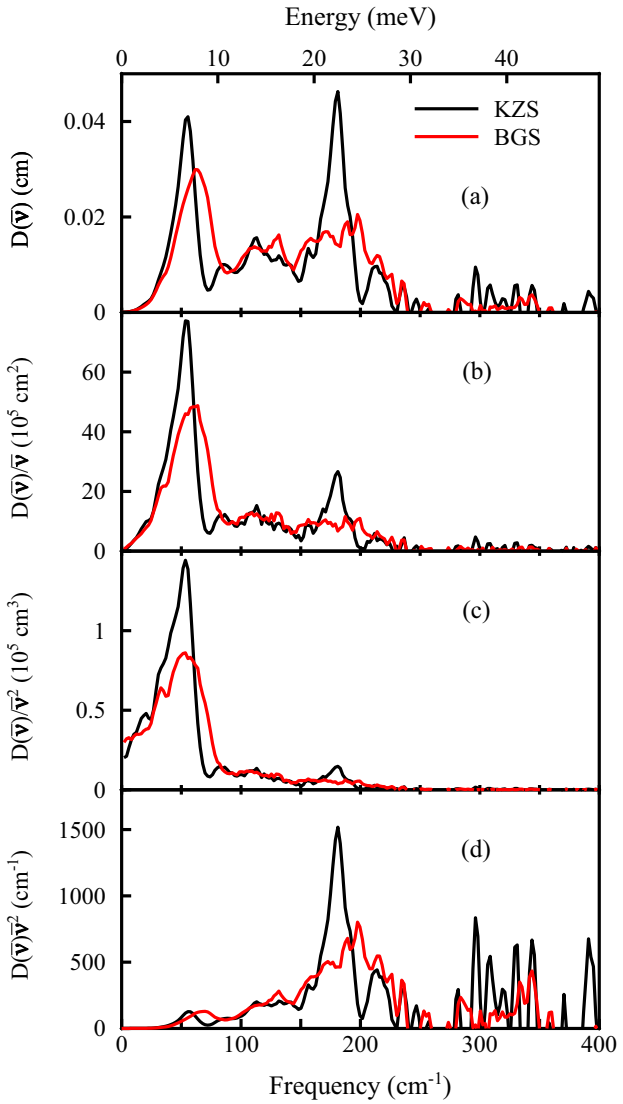

FIG. 8. (Color online) NRIXS data for KZS and BGS shown in terms of $D(\bar{\nu})$, $D(\bar{\nu})/\bar{\nu}$, $D(\bar{\nu})/\bar{\nu}^2$, and $D(\bar{\nu})\bar{\nu}^2$ to emphasize the vibrational modes that have the main contribution to the low-[Eq. (4)] and high-[Eq. (3)] temperature limiting values for Sn msd, and to the stiffness [Eq. (6)].

in the values for the Sn resilience and, consequently, in the temperature dependence of the msd.

In addition to the slight shift to higher frequencies of the dominant feature below 100 cm^{-1} in BGS with respect to KZS, the 150–220 cm^{-1} region in the two spectra look different as well [Fig. 8(a)], as discussed above. We introduce the concept of "stiffness" [40], an effective force constant determined by the Sn VDOS probing the strength of the nearest neighbor interactions with Sn [49]:

$$k_s = m_{\mathrm{Sn}} \frac{(2\pi c)^2}{3} \int D(\bar{\nu})\bar{\nu}^2 d\bar{\nu}, \qquad (6)$$

where m_{Sn} is the mass of the Sn atom. The factor of 3 is due to an averaging over all directions for the isotropic samples considered here. In order to emphasize the dominant contribution of the 150–220 cm^{-1} frequency region to the stiffness, in Fig. 8(d), we plot the integrand in Eq. (6). On the other hand, lower-frequency modes, which, as we have seen, contribute significantly to the resilience, do not have a major effect on the stiffness.

TABLE II. Select structural information for KZS and BGS (Refs. [31,33] and this work [34]), and elastic and thermodynamic properties extracted from Sn VDOS.

	KZS	BGS
Unit-cell volume (Å^3)	1759.1	1549.8
Average Sn-neighbor bond length (Å)	2.791	2.715
Resilience (N/m)	36.4 ± 0.5	39.5 ± 0.6
Stiffness (N/m)	127.9 ± 2	136.1 ± 2
Vibrational isochoric specific heat (k_B/atom)	2.9	2.9
Vibrational entropy (k_B/atom)	5	5
Vibrational energy (meV/atom)	79.8	79.9

Given the correlation between bond length and frequency [55] on one hand, and between frequency and stiffness [Eq. (6)] on the other, it is expected that stiffness monitors subtle changes in the bond lengths between Sn and its neighbors, similar to those of the Fe atom in proteins [47,49,56]. Indeed, the larger KZS unit cell compared to the BGS one (and, consequently, the larger average Sn-neighboring atom bond length) translates into a smaller value for the stiffness for KZS with respect to BGS (Table II). To put the stiffness values for KZS and BGS in perspective, the mean force constant of the Fe environment in a filled skutterudite ($CeFe_4Sb_{12}$) is 202 N/m at 295 K [29]. In the same study, a downshift of about 4 cm^{-1} was observed in the positions of the main peaks in the Fe VDOS of $EuFe_4Sb_{12}$ compared to $CeFe_4Sb_{12}$, consistent with the larger unit-cell volume of the Eu-filled compound. Knowing the actual value of the stiffness may prove particularly useful in the research involving the mechanical properties of clathrates [3].

With the benefit of hindsight, Raman spectra could actually predict the relative resilience and stiffness values for various compounds. The dominant band around 60 cm^{-1} dictates the resilience, i.e., the temperature dependence of the thermal fluctuations of the Sn atoms in the host framework. On the other hand, the band around 175 cm^{-1} is sensitive to subtle changes in the bond lengths between Sn atoms and its neighbors and, ultimately, to differences in the molecular size. As noted before, despite its relative richness in KZS compared to BGS, the 80–160 cm^{-1} region plays a smaller role in the overall dynamics of the host framework compared to other regions of the spectrum (Fig. 8). Due to the high similarities between the Raman and NRIXS spectra, one can use the former to compare *qualitatively* the stiffness of various compounds. For example, the highest frequency bands in the Raman spectra of Ge (Sn)-based compounds appear around 250 (200) cm^{-1} [42], suggesting a higher stiffness for the Ge-containing frameworks compared to the Sn ones [Eq. (6)]. This result is in agreement with previous studies, in which the high rigidity of Ga/Ge systems was demonstrated by EXAFS studies [57], while diffraction measurements on $Sr_8Ga_{16}Ge_{30}$ [58] and BGS [33] revealed atomic displacement parameters for the Ge compound about twice smaller than for the Sn one.

Furthermore, several thermodynamic properties can be calculated from the partial VDOS, such as the internal energy per atom, the lattice specific heat per atom at constant volume, and the vibrational entropy per atom [24,25]. Their values at 298 K are listed in Table II. Again, these quantities give the contribution of only the Sn atoms and may be used in parallel with theoretical calculations [45] to obtain a complete picture of the thermodynamic behavior of the material.

To conclude, we performed a joint Sn-based NRIXS/Raman study on two promising thermoelectric materials, Zintl clathrates $K_8Zn_4Sn_{42}$ and $Ba_8Ga_{16}Sn_{30}$. The ultimate selectiveness of NRIXS and its highly quantitative nature allowed us to specifically probe the host frameworks in these compounds without interference from the guest atoms. As expected, Raman and NRIXS spectra are very similar and they are both sensitive to subtle structural differences. NRIXS, however, provides a series of elastic and thermodynamic quantities not available from Raman, thus opening an avenue for systematic NRIXS studies on Sn-based clathrates that may reveal important connections between their thermoelectric [35,59,60], magnetic [61], and mechanical [62] properties and the physical properties of the host framework. For example, recent NRIXS work [30] on skutterudites showed that the Fe_4Sb_{12} framework is softer than the Co_4Sb_{12} one, indicating that, in addition to the filler, the framework plays an important role in the lattice thermal conductivity. Similarly, NRIXS has the potential of becoming a useful tool in the endeavor of finding and characterizing new materials that fulfill the "phonon glass, electron crystal" requirement or for other applications, whether on its own or in combination with more established techniques.

ACKNOWLEDGMENTS

This research used resources of the Advanced Photon Source, a U.S. Department of Energy (DOE) Office of Science User Facility operated for the DOE Office of Science by Argonne National Laboratory under Contract No. DE-AC02-06CH11357. This work was performed, in part, at the Center for Nanoscale Materials, a U.S. DOE, Office of Science, Office of Basic Energy Sciences User Facility under Contract No. DE-AC02-06CH11357.

[1] A. V. Shevelkov and K. Kovnir, Struct. Bond. **139**, 97 (2011).
[2] M. Christensen, S. Johnsen, and B. B. Iversen, Dalton Trans. **39**, 978 (2010).
[3] A. San-Miguel, P. Kéghélian, X. Blase, P. Mélinon, A. Perez, J. P. Itié, A. Polian, E. Reny, C. Cros, and M. Pouchard, Phys. Rev. Lett. **83**, 5290 (1999).
[4] Y. Li and J. H. Ross, Jr., Appl. Phys. Lett. **83**, 2868 (2003).
[5] H. Kawaji, H.-o. Horie, S. Yamanaka, and M. Ishikawa, Phys. Rev. Lett. **74**, 1427 (1995).
[6] A. D. Martinez, L. Krishna, L. L. Baranowski, M. T. Lusk, E. S. Toberer, and A. C. Tamboli, IEEE J. Photovolt. **3**, 1305 (2013).
[7] M. Beekman and G. S. Nolas, J. Mater. Chem. **18**, 842 (2008).
[8] K. Tanigaki, T. Shimizu, K. M. Itoh, J. Teraoka, Y. Moritomo, and S. Yamanaka, Nat. Mater. **2**, 653 (2003).
[9] G. A. Slack, in *CRC Handbook of Thermoelectrics*, edited by D. M. Rowe (CRC Press, Boca Raton, FL, 1995), Chap. 34, p. 407.
[10] B. C. Sales, D. Mandrus, and R. K. Williams, Science **272**, 1325 (1996).
[11] B. C. Sales, D. Mandrus, B. C. Chakoumakos, V. Keppens, and J. R. Thompson, Phys. Rev. B **56**, 15081 (1997).
[12] G. S. Nolas, T. J. R. Weakley, and J. L. Cohn, Chem. Mater. **11**, 2470 (1999).
[13] R. P. Hermann, W. Schweika, O. Leupold, R. Rüffer, G. S. Nolas, F. Grandjean, and G. J. Long, Phys. Rev. B **72**, 174301 (2005).
[14] M. Christensen, F. Juranyi, and B. B. Iversen, Physica B **385-386**, 505 (2006).
[15] J. Dong and O. F. Sankey, J. Phys.: Condens. Matter **11**, 6129 (1999).
[16] C. W. Myles, J. Dong, O. F. Sankey, C. A. Kendziora, and G. S. Nolas, Phys. Rev. B **65**, 235208 (2002).
[17] M. Christensen, A. B. Abrahamsen, N. B. Christensen, F. Juranyi, N. H. Andersen, K. Lefmann, J. Andreasson, C. R. H. Bahl, and B. B. Iversen, Nat. Mater. **7**, 811 (2008).
[18] S. Christensen, L. Bjerg, A. Kaltzoglou, F. Juranyi, T. Fässler, T. Unruh, and M. Christensen, J. Appl. Phys. **113**, 084902 (2013).
[19] M. Stordeur, in *CRC Handbook of Thermoelectrics* edited by D. M. Rowe (CRC Press, Boca Raton, FL, 1995), Chap. 20, p. 239.
[20] E. Reny, A. San-Miguel, Y. Guyot, B. Masenelli, P. Mélinon, L. Saviot, S. Yamanaka, B. Champagnon, C. Cros, M. Pouchard, M. Borowski, and A. J. Dianoux, Phys. Rev. B **66**, 014532 (2002).
[21] H. Shimizu, T. Imai, T. Kume, S. Sasaki, A. Kaltzoglou, and T. F. Fässler, Chem. Phys. Lett. **464**, 54 (2008).
[22] A. Kaltzoglou, T. F. Fässler, C. Gold, E.-W. Scheidt, W. Scherer, T. Kume, and H. Shimizu, J. Solid State Chem. **182**, 2924 (2009).
[23] R. Lortz, R. Viennois, A. Petrovic, Y. Wang, P. Toulemonde, C. Meingast, M. M. Koza, H. Mutka, A. Bossak, and A. San Miguel, Phys. Rev. B **77**, 224507 (2008).
[24] R. Rüffer and A. I. Chumakov, Hyperfine Interact. **128**, 255 (2000).
[25] W. Sturhahn, J. Phys.: Condens. Matter **16**, S497 (2004).
[26] J. T. Sage, C. Paxson, G. R. A. Wyllie, W. Sturhahn, S. M. Durbin, P. M. Champion, E. E. Alp, and W. R. Scheidt, J. Phys.: Condens. Matter **13**, 7707 (2001).
[27] J. S. Tse, D. D. Klug, J. Y. Zhao, W. Sturhahn, E. E. Alp, J. Baumert, C. Gutt, M. R. Johnson, and W. Press, Nat. Mater. **4**, 917 (2005).
[28] D. D. Klug, J. S. Tse, J. Y. Zhao, W. Sturhahn, E. E. Alp, and C. A. Tulk, Phys. Rev. B **83**, 184116 (2011).
[29] G. J. Long, R. P. Hermann, F. Grandjean, E. E. Alp, W. Sturhahn, C. E. Johnson, D. E. Brown, O. Leupold, and R. Rüffer, Phys. Rev. B **71**, 140302 (2005).
[30] A. Möchel, I. Sergueev, N. Nguyen, G. J. Long, F. Grandjean, D. C. Johnson, and R. P. Hermann, Phys. Rev. B **84**, 064302 (2011).

[31] V. Baran, A. Fischer, W. Scherer, and T. F. Fässler, Z. Anorg. Allg. Chem. **639**, 2125 (2013).
[32] M. A. Kirsanova and A. V. Shevelkov, Z. für Kristall. **228**, 215 (2013).
[33] D. Huo, T. Sakata, T. Sasakawa, M. A. Avila, M. Tsubota, F. Iga, H. Fukuoka, S. Yamanaka, S. Aoyagi, and T. Takabatake, Phys. Rev. B **71**, 075113 (2005).
[34] See Supplemental Material at http://link.aps.org/supplemental/10.1103/PhysRevB.90.104304 for details on sample preparation and characterization, and additional NRIXS results.
[35] M. A. Avila, K. Suekuni, K. Umeo, H. Fukuoka, S. Yamanaka, and T. Takabatake, Appl. Phys. Lett. **92**, 041901 (2008).
[36] T. S. Toellner, A. Alatas, and A. H. Said, J. Synchrotron Rad. **18**, 605 (2011).
[37] B. Roldan Cuenya, W. Keune, W. Sturhahn, T. S. Toellner, and M. Y. Hu, Phys. Rev. B **64**, 235321 (2001).
[38] H. Giefers, S. Koval, G. Wortmann, W. Sturhahn, E. E. Alp, and M. Y. Hu, Phys. Rev. B **74**, 094303 (2006).
[39] T. S. Toellner, M. Y. Hu, G. Bortel, W. Sturhahn, and D. Shu, Nucl. Instrum. Methods Phys. Res. Sect. A **557**, 670 (2006).
[40] H. J. Lipkin, Phys. Rev. B **52**, 10073 (1995).
[41] W. Sturhahn, Hyperfine Interact. **125**, 149 (2000).
[42] G. S. Nolas and C. A. Kendziora, Phys. Rev. B **62**, 7157 (2000).
[43] H. Shimizu, R. Oe, S. Ohno, T. Kume, S. Sasaki, K. Kishimoto, T. Koyanagi, and Y. Ohishi, J. Appl. Phys. **105**, 043522 (2009).
[44] T. Imai, T. Kume, S. Sasaki, H. Shimizu, A. Kaltzoglou, and T. F. Fässler, J. Phys. Chem. Solids **71**, 587 (2010).
[45] P. Norouzzadeh, C. W. Myles, and D. Vashaee, J. Appl. Phys. **114**, 163509 (2013).
[46] M. S. Diakhate, R. P. Hermann, A. Möchel, I. Sergueev, M. Søndergaard, M. Christensen, and M. J. Verstraete, Phys. Rev. B **84**, 125210 (2011).
[47] Y. Xiao, H. Wang, S. J. George, M. C. Smith, M. W. W. Adams, F. E. Jenney, Jr., W. Sturhahn, E. E. Alp, J. Zhao, Y. Yoda, A. Dey, E. I. Solomon, and S. P. Cramer, J. Am. Chem. Soc. **127**, 14596 (2005).
[48] W. Zeng, N. J. Silvernail, D. C. Wharton, G. Y. Georgiev, B. M. Leu, W. R. Scheidt, J. Zhao, W. Sturhahn, E. E. Alp, and J. T. Sage, J. Am. Chem. Soc. **127**, 11200 (2005).
[49] B. M. Leu, T. H. Ching, J. Zhao, W. Sturhahn, E. E. Alp, and J. T. Sage, J. Phys. Chem. B **113**, 2193 (2009).
[50] A. A. Maradudin, E. W. Montroll, G. H. Weiss, and I. P. Ipatova, *Theory of Lattice Dynamics in the Harmonic Approximation*, 2nd ed. (Academic Press, New York, 1971), Chap. IV, p. 129.
[51] M. Y. Hu, T. S. Toellner, N. Dauphas, E. E. Alp, and J. Zhao, Phys. Rev. B **87**, 064301 (2013).
[52] A. I. Chumakov, A. Barla, R. Rüffer, J. Metge, H. F. Grünsteudel, H. Grünsteudel, J. Plessel, H. Winkelmann, and M. M. Abd-Elmeguid, Phys. Rev. B **58**, 254 (1998).
[53] B. M. Leu, Y. Zhang, L. Bu, J. E. Straub, J. Zhao, W. Sturhahn, E. E. Alp, and J. T. Sage, Biophys. J. **95**, 5874 (2008).
[54] G. Zaccai, Science **288**, 1604 (2000).
[55] R. M. Badger, J. Chem. Phys. **2**, 128 (1934).
[56] W. Zeng, A. Barabanschikov, Y. Zhang, J. Zhao, W. Sturhahn, E. E. Alp, and J. T. Sage, J. Am. Chem. Soc. **130**, 1816 (2008).
[57] R. Baumbach, F. Bridges, L. Downward, D. Cao, P. Chesler, and B. Sales, Phys. Rev. B **71**, 024202 (2005).
[58] L. Qiu, I. P. Swainson, G. S. Nolas, and M. A. White, Phys. Rev. B **70**, 035208 (2004).
[59] J. V. Zaikina, K. A. Kovnir, A. V. Sobolev, I. A. Presniakov, Y. Prots, M. Baitinger, W. Schnelle, A. V. Olenev, O. I. Lebedev, G. Van Tendeloo, Y. Grin, and A. V. Shevelkov, Chem. - Eur. J. **13**, 5090 (2007).
[60] M. C. Schäfer and S. Bobev, J. Am. Chem. Soc. **135**, 1696 (2013).
[61] J. V. Zaikina, W. Schnelle, K. A. Kovnir, A. V. Olenev, Y. Grin, and A. V. Shevelkov, Solid State Sci. **9**, 664 (2007).
[62] A. J. Karttunen, V. J. Härkönen, M. Linnolahti, and T. A. Pakkanen, J. Phys. Chem. C **115**, 19925 (2011).